

Original Research

A glypican-1-targeted antibody-drug conjugate exhibits potent tumor growth inhibition in glypican-1-positive pancreatic cancer and esophageal squamous cell carcinoma ☆, ☆, ☆, ☆

Eri Munekegawa^{1,2}; Satoshi Serada^{2,3,*}; Shigehiro Tsujii^{1,2}; Keiichiro Yokota^{1,2}; Keita Kiuchi⁴; Kenji Tominaga⁴; Minoru Fujimoto^{2,5}; Mizuki Kanda³; Sunao Uemura¹; Tsutomu Namikawa¹; Taisei Nomura⁶; Ichiro Murakami⁷; Kazuhiro Hanazaki¹; Tetsuji Naka^{2,3,5,*}



¹ Department of Surgery, Kochi University, Nankoku, Kochi, Japan

² Department of Clinical Immunology, Kochi Medical School, Kochi University, Nankoku, Kochi, Japan

³ Institute for Biomedical Sciences Molecular Pathophysiology, Iwate Medical University, Yahaba, Iwate, Japan

⁴ Department of Medical course, Kochi Medical School, Kochi University, Nankoku, Kochi, Japan

⁵ Division of Allergy and Rheumatology, Department of Internal Medicine, Iwate Medical University School of Medicine, Yahaba, Iwate, Japan

⁶ Animal Models of Human Diseases, National Institute of Biomedical Innovation, Health and Nutrition, Ibaraki, Osaka, Japan

⁷ Department of Pathology, School of Medicine, Kochi University, Nankoku, Kochi, Japan

Abstract

An antibody-drug conjugate (ADC) is a promising therapeutic modality because selective and effective delivery of an anti-cancer drug is achieved by drug-conjugated antibody-targeting cancer antigen. Glypican 1 (GPC1) is highly expressed in malignant tumors, including pancreatic ductal adenocarcinoma (PDAC) and esophageal squamous cell carcinoma (ESCC). Herein, we describe the usefulness of GPC1-targeting ADC. Humanized anti-GPC1 antibody (clone T2) was developed and conjugated with monomethyl auristatin E (MMAE) via maleimidocaproyl-valine-citrulline-p-aminobenzyloxycarbonyl (mc-vc-PABC) linkers (humanized GPC1-ADC[MMAE]). Humanized GPC1-ADC(MMAE) inhibited the growth of GPC1-positive PDAC and ESCC cell lines via inducing cycle arrest in the G2/M phase and apoptosis in vitro. The binding activity of humanized GPC1-ADC(MMAE) with GPC1 was comparable with that of the unconjugated anti-GPC1 antibody. The humanized GPC1-ADC(MMAE) was effective in GPC1-positive BxPC-3 subcutaneously xenografted mice but not in GPC1-negative BxPC-3-GPC1-KO xenografted mice. To assess the bystander killing activity of the humanized GPC1-ADC(MMAE), a mixture of GPC1-positive BxPC-3 and GPC1-negative BxPC-3-GPC1-KO-Luc cells were subcutaneously inoculated, and a heterogenous GPC1-expressing tumor model was developed. The humanized GPC1-ADC(MMAE) inhibited the tumor growth and decreased the luciferase signal, measured with an in vivo imaging system (IVIS), which suggests that the suppression of the BxPC-3-GPC1-KO-Luc population. The humanized GPC1-ADC(MMAE) also inhibited the established liver metastases of BxPC-3 cells and significantly improved the overall survival of the mice. It exhibited a potent antitumor effect on the GPC1-positive PDAC and ESCC patient-derived xenograft (PDX) models. Our preclinical data demonstrate that GPC1 is a promising therapeutic target for ADC.

Neoplasia (2021) 23, 939–950

Keywords: Antibody-drug conjugate, Glypican-1, Pancreatic cancer, Esophageal squamous cell carcinoma

* Corresponding authors.

E-mail addresses: serada@kochi-u.ac.jp (S. Serada), naka@kochi-u.ac.jp (T. Naka).

☆ *Abbreviations:* BLI, bioluminescence imaging; mAb, monoclonal antibody; mAbs, monoclonal antibodies; MMAE, monomethyl auristatin E; PDAC, pancreatic ductal adenocarcinoma; PDX, patient-derived tumor xenograft; SPR, surface plasmon resonance

☆☆ *Funding:* This research was supported by Japan Agency for Medical Research and Development (AMED) under Grant No. JP18lm0203068, JP21ck0106650, and the JSPS KAKENHI Grant Numbers JP16K07193 and JP19K07732.

* *Conflict of interest:* S.S., M.F., and T.N. declare a patent for US10077316B2 issued and a patent for WO2015098112A1 pending related to the anti-GPC1 monoclonal antibody.

Introduction

While cancer survival has improved, the prognosis of some cancers remains poor. Pancreatic ductal adenocarcinoma (PDAC) is one of the most lethal malignant neoplasms across the world and is the seventh leading cause of cancer-related deaths [1]. The incidence of PDAC is increasing worldwide and is expected to become the second leading cause of cancer-related death by 2030 [2]. As PDAC is asymptomatic until it progresses, only 20% of cases can be resected at diagnosis, and more than half are found at stage IV, with an overall 5-year survival rate of only 6% [3]. Esophageal squamous cell carcinoma (ESCC) is the sixth leading cause of death from cancer. The number of patients with ESCC is increasing worldwide and is expected to increase by approximately 35% from 2018 to 2030 [4]. Similar to that of PDAC, the diagnosis of ESCC is often delayed, and the 5-year survival rate is $\leq 20\%$, with a poor prognosis. Therefore, there is an urgent need for the development of a new effective treatment method for such intractable cancer.

An antibody-drug conjugate (ADC) is a topical targeted therapeutic agent that uses immunoconjugate in which anti-cancer drugs are chemically or enzymatically bound to monoclonal antibodies (mAb). ADC can deliver a highly cytotoxic payload to cancer cells by binding to cancer-specific antigens. This platform enables targeting cancer cells and selective delivery of highly cytotoxic drugs, resulting in a broad therapeutic window. Since the approval of brentuximab vedotin (Adcetris) in 2011 for CD30-positive lymphomas [5,6] and trastuzumab emtansine (Kadcyla) in 2013 for Her2-positive breast cancer [7-9], ADCs have received increasing attention. Boosted by success stories, >50 different ADCs are in clinical development. Recently, our group identified glypican 1 (GPC1) as a novel cancer antigen in ESCC by a quantitative protein expression profiling analysis focused on plasma membrane proteins [10]. GPC1 is a heparan sulfate proteoglycan that binds to the plasma membrane by a glycosylphosphatidylinositol anchor [11,12]. It has been reported that GPC1 promoted tumor growth, metastasis, and invasion by acting as a coreceptor, enhancing various signaling pathways, such as Wnt, Hedgehog, transforming growth factor- β , and fibroblast growth factor-2 [13,14]. Elevated GPC1 expression level has been reported in breast cancer, glioblastoma, uterine cervical cancer, and PDAC [15-18]. Furthermore, GPC1 is also expressed in metastatic lymph nodes in ESCC [14]. GPC1 expression in normal tissues is mainly restricted to the testis or ovary, unlike ESCC tissues [14].

We previously demonstrated that the microtubule-disrupting agent monomethyl auristatin F (MMAF) conjugated to mouse anti-GPC1 monoclonal antibody (clone 01a033) was effective against GPC1-positive cervical cancer and PDAC preclinical models [17,19]. The aims of this study were to develop a novel humanized GPC1-ADC and assess the antitumor effect of humanized GPC1-ADC and show GPC1 as a promising therapeutic target for PDAC and ESCC.

In this study, we generated a novel humanized anti-GPC1 antibody conjugated with the potent microtubule-disrupting agent MMAE that has a bystander killing activity [20,21]. After the cleavage of the peptide linker within the first internalized tumor cell, released MMAE can enter nearby tumor cells, including GPC1-negative tumor cells and damaged cells, which is called the “bystander killing effect.” A series of experiments of detailed preclinical characterization both *in vitro* and *in vivo* revealed that this humanized GPC1-ADC(MMAE) is highly selective and shows potent *in vivo* efficacy in several xenografts and patient-derived tumor xenograft (PDX) models of PDAC and ESCC.

Materials and methods

Cell lines and culture

Two human pancreatic cancer cell lines, namely BxPC-3 (RRID:CVCL_0186) and PK-8 (RRID:CVCL_4718) were obtained from the European Collection of Authenticated Cell Cultures, the Japanese Collection of Research Bioresources (Osaka, Japan), and RIKEN BioResource Center (Wako, Japan), respectively. The human ESCC cell lines TE-8 (RRID:CVCL_1766) and TE-14 (RRID:CVCL_3336) were obtained from the RIKEN BioResource Center. Human pancreatic cancer cell line KP-2 (RRID:CVCL_3004) and human ESCC cell line KYSE70 (RRID:CVCL_1356) were obtained from the Japanese Collection of Research Bioresources (Osaka, Japan). BxPC-3-Luc#2 was obtained from the Japanese Collection of Research Bioresources (Osaka, Japan). BxPC-3 and BxPC-3-Luc#2 were maintained in Roswell Park Memorial Institute (RPMI) 1640 medium supplemented with 10% fetal bovine serum (FBS; Thermo Fisher Scientific Inc., Waltham, MA, USA), 1% GlutaMAX (Thermo Fisher Scientific), 100 U/ml penicillin, and 100 $\mu\text{g}/\text{ml}$ streptomycin (Nacalai Tesque). KP-2, PK-8, TE-8, and TE-14 were maintained in RPMI 1640 medium supplemented with 10% FBS, 100 U/ml penicillin, and 100 $\mu\text{g}/\text{ml}$ streptomycin. KYSE70 was maintained in Ham's F12/RPMI1640 medium supplemented with 20% FBS, 100 U/ml penicillin, and 100 $\mu\text{g}/\text{ml}$ streptomycin. The cultures were maintained at 37°C in a humidified atmosphere at 5% CO₂. The identity of each cell line was confirmed by DNA fingerprinting using short tandem repeat (STR) profiling, as previously described [22]. All cells were tested negative for Mycoplasma with the use of a MycoAlert Mycoplasma Detection Kit (Lonza) and used less than 3 months after resuscitation.

Generation of anti-GPC1 antibodies

Generation of the mouse anti-human GPC1 antibody (clone 01a033) was previously described [17]. To humanize mouse anti-human GPC1 antibody (clone 01a033), a human VK library was constructed with a fixed heavy chain of murine antibody CDRs and human framework, followed by antigen panning and screening. A total of 30 humanized anti-GPC1 antibodies were discovered from the panning of the VK library and confirmed by phage enzyme-linked immunosorbent assay. Twenty of the antibodies were picked for antibody expression and purification, followed by affinity determination using Biacore 8K. Humanized antibodies were produced as a subclass of human IgG4, and mouse/human chimeric anti-GPC1 antibody (clone 01a033) was also produced. VL and VH sequences were analyzed to sort out unique hits and determine hit diversity.

Generation of humanized GPC1-ADC

The humanized anti-GPC1 antibody T2 was conjugated to auristatin MMAE by using previously described methods [23]. The human IgG4 isotype control recombinant antibody (clone QA16A1) was purchased from BioLegend, and the control IgG-ADC (control-ADC) was synthesized using the same method as that used for the humanized GPC1-ADC(MMAE). The drug-to-antibody ratio (DAR) was 4.01 for humanized GPC1-ADC(MMAE) and was 4.17 for control-ADC, determined with hydrophobic interaction chromatography.

Immunohistochemistry

Formalin-fixed, paraffin-embedded tissue sections of 5 μm in size for pancreatic cancer primary and matched metastatic tissue microarray were obtained from Tristar Technology Group (Bethesda, MD, USA). The GPC1

Received 20 May 2021; received in revised form 10 July 2021; accepted 12 July 2021

expression in tumor tissues was evaluated using a rabbit polyclonal anti-GPC1 antibody (1:2,000, catalog No. GTX104557; GeneTex, San Antonio, TX, USA) and visualized using Envision ChemMate (Dako, Glostrup, Denmark) according to the manufacturer's instructions. Stained sections were also photographed using phase-contrast light microscopy (DM2500 with Leica Application Suite version 3.80; Leica Microsystems GmbH, Wetzlar, Germany).

Statistical analyses

Data are shown as mean \pm SD for the *in vitro* experiments and mean \pm SEM for the *in vivo* experiments. For the comparisons between the two groups, data were analyzed using the Student *t*-test. For comparisons among three or more groups, data were analyzed using one-way analysis of variance, followed by Dunnett's *post hoc* test. Differences were considered significant at $P < 0.05$.

Other experiments are described in the Supporting Information Methods.

Results

Preparation of a humanized GPC1-ADC

As previously described, mouse anti-human GPC1 antibody (clone 01a033) showed high internalizing activity and usefulness for ADC [17,19]. To develop a humanized anti-human GPC1 antibody, a human VK library was constructed using a fixed heavy chain of murine antibody CDRs with a human framework, and antigen panning and screening were performed. Among the discovered humanized anti-GPC1 antibodies, 20 were selected for affinity determination using surface plasmon resonance. Among 20 clones, clone T2 showed better affinity (K_D , 5.20 nM) than the mouse/human chimeric anti-GPC1 mAb clone (K_D , 10.2 nM; Supplementary Table 1). To identify the optimal mAb for a GPC1-targeting ADC, 20 clones were screened on the basis of their ability to deliver an auristatin payload into GPC1-expressing cells *in vitro* by using an indirect cytotoxicity assay exposing cells to a humanized anti-GPC1 mAb and MMAF-conjugated secondary antibody. Among 20 mAbs, clone T2 most efficiently delivered the MMAF-conjugated secondary antibody into the GPC1-positive cells (Supplementary Table 2). According to these results, we selected clone T2 for the antibody component of the humanized GPC1-ADC.

To confirm the expression of GPC1 in pancreatic cancer and ESCC cell lines, a flow cytometric analysis was performed using a humanized anti-GPC1 antibody clone T2. The pancreatic cancer cell lines (BxPC-3, KP-2, and PK-8) and ESCC cell lines (TE8, TE14, and KYSE70) showed high GPC1 expression levels, while the GPC1 expression was not detected in the GPC1-knockout cell lines (BxPC-3-GPC1-KO and TE8-GPC1-KO) generated by the CRISPR-Cas9 system (Fig. 1A). The GPC1 knockout was also confirmed with western blot analysis (Supplementary Fig. 1).

Humanized anti-GPC-1 mAb (clone T2) or an isotype control human IgG4 was conjugated via the protease-sensitive linker maleimidocaproyl-valine-citrulline-*p*-aminobenzyloxycarbonyl (mc-vc-PABC) to the auristatin MMAE (Fig. 1B). The DAR was 4.0 for humanized GPC1-ADC(MMAE) and 4.2 for control-ADC(MMAE). In the flow cytometric analysis, MMAE conjugation did not affect the antibody-binding activity against BxPC-3 (unconjugated humanized anti-GPC1 mAb: $K_D = 0.529$ nM, binding max = 1,495; humanized GPC1-ADC(MMAE): $K_D = 0.570$ nM, binding max = 1,463; Fig. 1C).

Internalization of humanized GPC1-ADC was confirmed in the BxPC-3 cells

The binding capacity and percentage of internalization of the humanized anti-GPC1 mAb (clone T2) and humanized GPC1-ADC(MMAE) were

determined using flow cytometry in BxPC-3. GPC1 remaining on the cell surface was measured with flow cytometry after each exposure to humanized anti-GPC-1 mAb (clone T2) or humanized GPC1-ADC(MMAE) using biotin-labeled anti-GPC1 mAb (clone 02b006), which recognizes an epitope independent of that bound by clone T2. The internalization of the humanized anti-GPC-1 mAb (clone T2) or humanized GPC1-ADC(MMAE) rapidly occurred in BxPC-3 cells and in case of comparable activity (Fig. 1D).

To confirm the translocation of the humanized GPC1-ADC(MMAE) to lysosomes, we performed immunofluorescence analysis, which was also used to show humanized GPC1-ADC(MMAE) binding to the cell membranes when preincubated at 4°C before the internalization assay. When humanized GPC1-ADC(MMAE) exposed cells were incubated at 37°C for 4 h, humanized GPC1-ADC(MMAE) membrane staining was decreased, and humanized GPC1-ADC(MMAE) was found instead in the lysosomes, as evidenced by the overlap of staining for humanized GPC1-ADC(MMAE) and the lysosomal marker LAMP-1 (Fig. 1E). Unconjugated humanized anti-GPC1 mAb (clone T2) also represented a similar pattern to humanized GPC1-ADC(MMAE). These results suggest that humanized GPC1-ADC(MMAE) is first bound to the membrane of GPC1-expressing cells and is then internalized and translocated to the lysosomal compartment.

Humanized GPC1-ADC(MMAE) successfully inhibited the proliferation of GPC1-expressing cancer cells

Humanized GPC1-ADC(MMAE) caused a dose-dependent inhibition of cell viability in the GPC1-positive cancer cell lines *in vitro* (Fig. 2A). We did not observe any significant cytotoxic activity against all the cell lines treated with a control-ADC(MMAE). The IC_{50} values of the humanized GPC1-ADC(MMAE) for the GPC1-positive cell lines ranged from 0.0383 to 0.343 nM (Table 1). Conversely, humanized GPC1-ADC(MMAE) had no effect on BxPC-3-GPC1 and TE-8-GPC1 KO cells. The IC_{50} values of the humanized GPC1-ADC(MMAE) were not calculated for the BxPC-3-GPC1 and TE-8-GPC1 KO cells, as the 16-nM cell inhibitory rate of the humanized GPC1-ADC(MMAE) did not reach 50% (Fig. 2A). However, the naked antibody did not exhibit an antiproliferative activity *in vitro* against the BxPC-3 cells (data not shown). The IC_{50} values of MMAE against the cell lines ranged from 0.288 to 0.349 nM (Table 1).

Next, we examined whether humanized GPC1-ADC(MMAE) effects on the cell cycle and apoptosis. Humanized GPC1-ADC(MMAE) significantly increased the proportion of cells in G2/M phase, whereas control-ADC did not change the proportion of cells in each cycle (Fig. 2B). In addition, humanized GPC1-ADC(MMAE) caused a dose-dependent increase in caspase 3/7 activity compared to control-ADC(MMAE) (Fig. 2C). The hallmarks of classic apoptosis including activation of caspase 3 and cleavage of PARP were also detected (Fig. 2D). These data suggest that humanized GPC1-ADC(MMAE) induces cell cycle arrest in the G2/M phase and promotes apoptosis through caspase3/7 dependent pathway.

In vivo efficacy study of humanized GPC1-ADC(MMAE) in the BxPC-3 xenograft

To assess the antitumor effect of humanized GPC1-ADC(MMAE), we developed three types of xenograft mice subcutaneously implanted with BxPC-3 (GPC1 positive), BxPC-3-GPC1-KO-Luc#15 (GPC1 negative), and the co-inoculation of BxPC-3 and BxPC-3-GPC1-KO-Luc#15 to determine the bystander killing effect of the humanized GPC1-ADC(MMAE).

By IHC, the GPC1 expression was confirmed in the BxPC-3 xenograft tumor, while the GPC1 expression was not detected in the BxPC-3-GPC1-KO-Luc#15 xenograft tumor (Fig. 3A). In the xenograft tumor of the co-inoculated mice, a heterogenous GPC1 expression was observed (Fig. 3A).

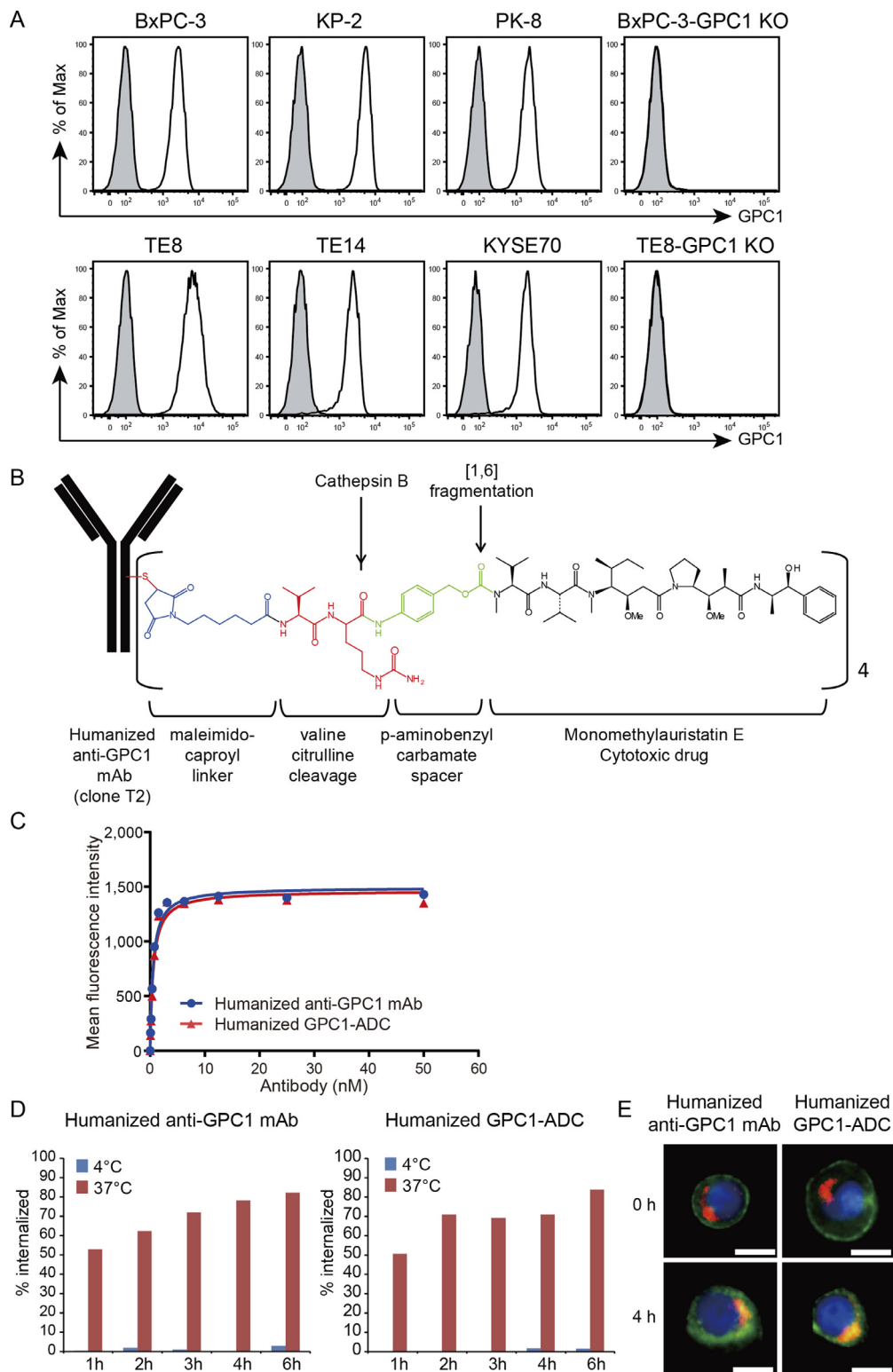


Fig. 1. Structure, characterization, and internalization activity of the humanized GPC1-ADC

A, Flow cytometric analysis of GPC1 expression. The shaded histogram profile indicates the isotype control, and the open histogram indicates the humanized anti-GPC1 antibody-staining results. B, Structure of the humanized GPC1-ADC consisting of the humanized anti-GPC1 antibody (clone T2) conjugated to the MMAE payload. C, BxPC-3 cells are incubated with unconjugated humanized anti-GPC1 mAb (blue closed circles) or humanized GPC1-ADC (red closed triangles). The mean fluorescence intensity at various concentrations is shown. D, Time-course analysis of the internalization activity of the antibody or ADC in BxPC-3 cells. The left panel shows unconjugated humanized anti-GPC1 mAb (clone T2); and the right panel, humanized GPC1-ADC. E, GPC1-ADC internalizes and locates in the lysosomes of BxPC-3 cells. Cell surface and intracellular GPC1 visualized on fluorescence microscopy. Green indicates the humanized anti-GPC1 antibody (clone T2) or humanized GPC1-ADC; red, the lysosomal marker LAMP-1; and blue, 4',6-diamidino-2-phenylindole-stained DNA. Scale bar: 10 mm. (Color version of figure is available online)

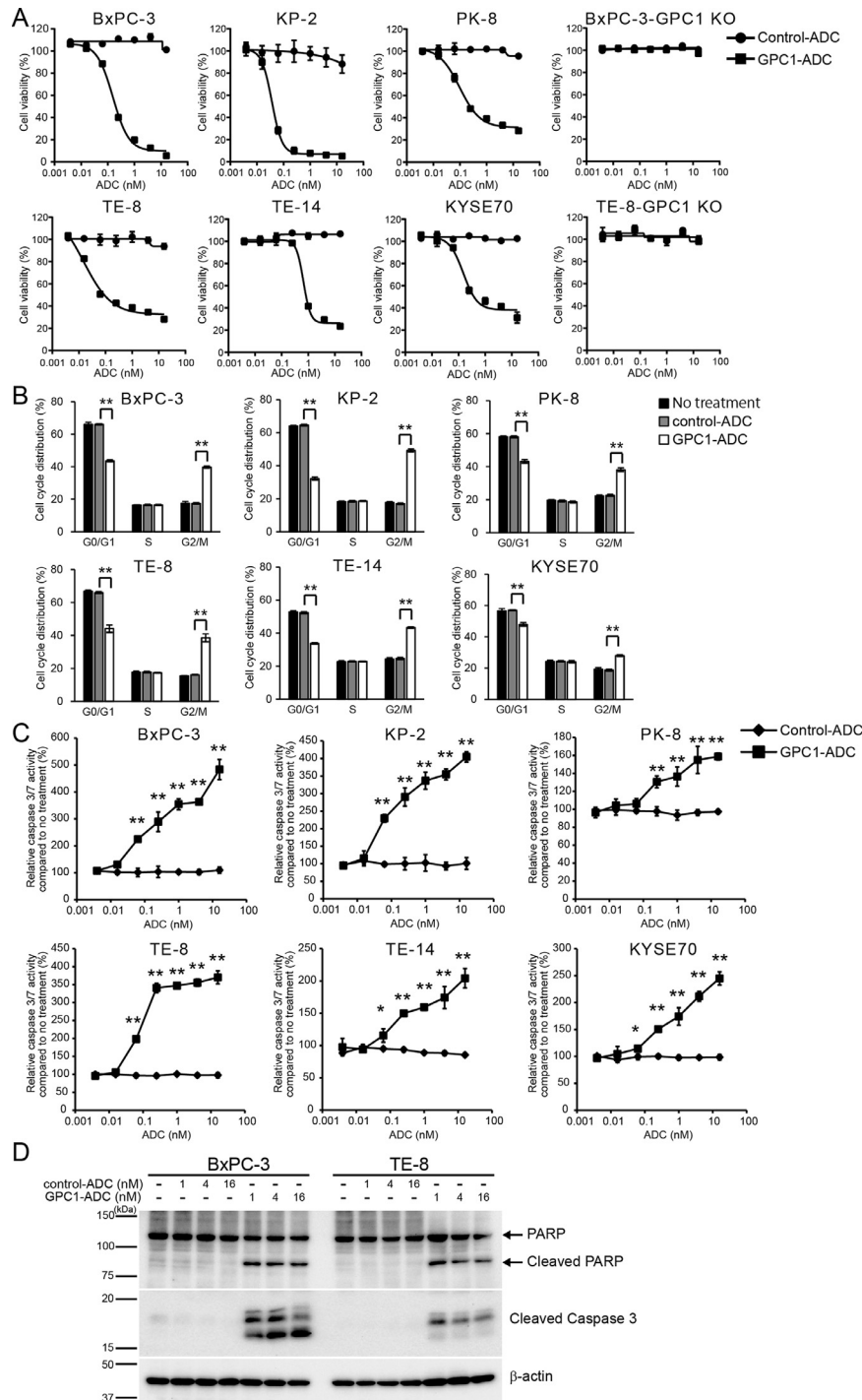


Fig. 2. *In vitro* cell growth inhibitory activity of ADC

A, Cancer cells were treated with humanized GPC1-ADC(MMAE) or human IgG4-ADC (a control-ADC[MMAE]) for 144 h. The humanized GPC1-ADC(MMAE) significantly inhibited the growth of the GPC1-positive cancer cell lines compared with the control-ADC(MMAE). In the GPC1-negative BxPC-3-GPC1 and TE8-GPC1 KO cell lines, neither treatment had any inhibitory effect. B, Induction of G2/M phase cell cycle arrest in BxPC-3, KP-2, PK-8, TE-8, TE-14, and KYSE70 cells treated with humanized GPC1-ADC(MMAE). Cells were treated with either 16 nM control-ADC(MMAE) or 16 nM humanized GPC1-ADC(MMAE). After 24 h, cell cycle analysis was performed by flow cytometry with propidium iodide DNA staining. $**P < 0.01$, by one-way ANOVA, followed by Dunnett's post hoc test. C, Induction of apoptosis in BxPC-3, KP-2, PK-8, TE-8, TE-14, and KYSE70 cells treated with 16 nM control-ADC(MMAE) or 16 nM humanized GPC1-ADC(MMAE). Caspase 3/7 activation was monitored using the Caspase Glo 3/7 assay system at 48 h after addition of ADCs. Caspase 3/7 activation relative to untreated cells was detected in these cells treated with increasing concentrations of humanized GPC1-ADC. $*P < 0.05$ and $**P < 0.01$, by Student's *t* test. D, Western blot analysis of proteins involved in the apoptosis pathways. BxPC-3 and TE-8 cells were treated with either 16 nM control-ADC(MMAE) or 16 nM humanized GPC1-ADC(MMAE). After 48 h, cells were harvested and lysed. The protein level of poly ADP-ribose polymerase (PARP), cleaved PARP, and Cleaved Caspase-3 was detected by western blot; β -actin was used as a loading control.

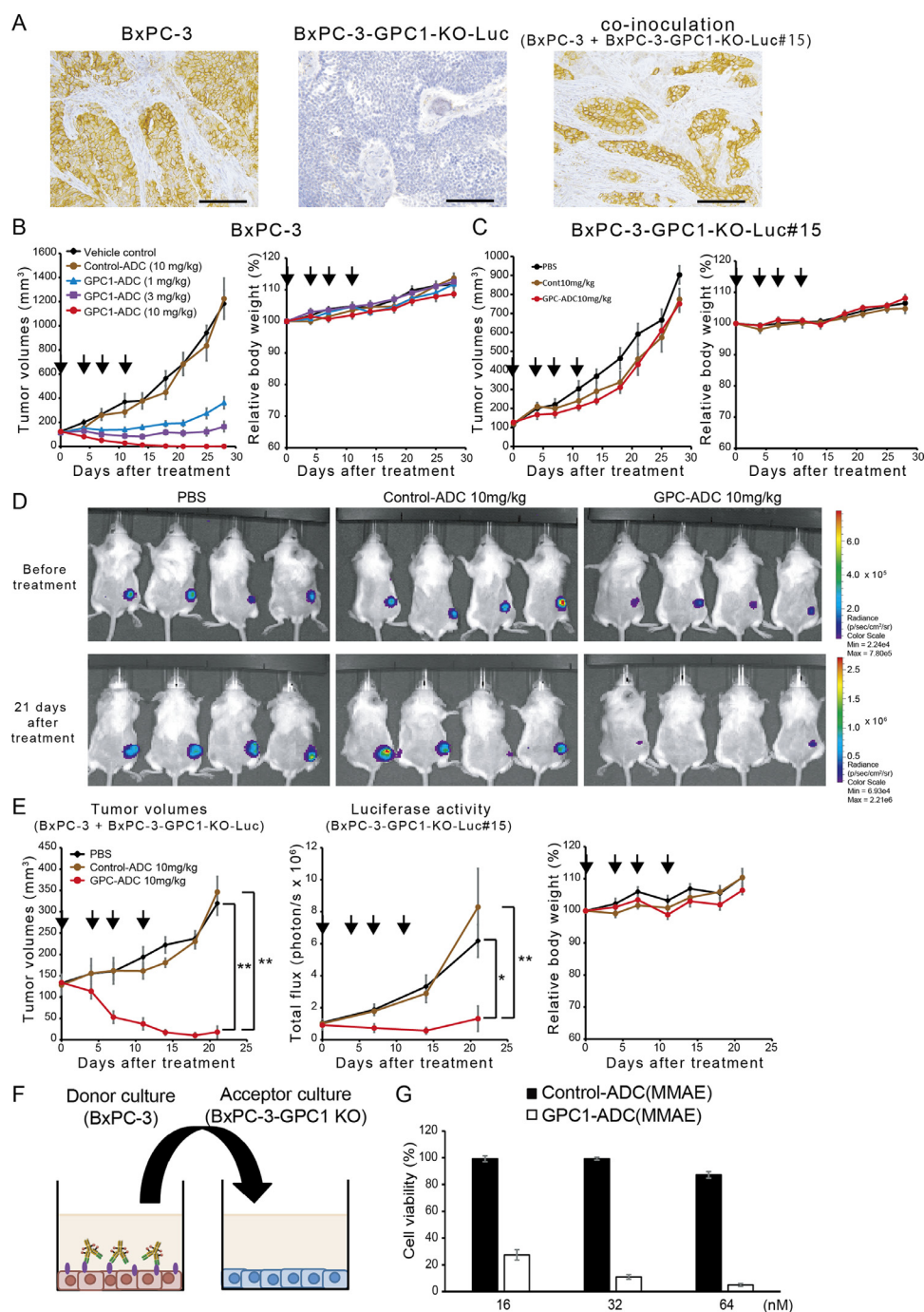


Fig. 3. Antitumor activity of the humanized GPC1-ADC(MMAE) *in vivo*
 A, Representative images of IHC staining for GPC1 in xenografted tumor tissues from BxPC-3, BxPC-3-GPC1-KO-Luc#15, and the co-inoculation of BxPC-3 and BxPC-3-GPC1-KO-Luc#15. Scale bar: 100 mm. B, Antitumor efficacy of the humanized GPC1-ADC(MMAE) in the BxPC-3 xenograft model (each $n = 7$ per group). Each point on the graph represents the average tumor volume. The changes in the relative body weight are represented. C, Antitumor efficacy of humanized GPC1-ADC(MMAE) in the BxPC-3-GPC1-KO-Luc#15 xenograft model (each $n = 7$ per group). Each point on the graph represents the average tumor volume. Changes in the relative body weight are also represented. D, Bystander killing effect of the humanized GPC1-ADC(MMAE) in the co-inoculated conditions *in vivo*. The time-course of the luciferase activity was detected by bioluminescence imaging (BLI) after the intraperitoneal administration of the substrate. The imaging data of the luciferase activity are shown in D. E, Tumor volumes are shown in the left panel. Quantification of the tumor burden from the BxPC-3-GPC1-KO-Luc#15 is shown in the middle panel. Changes in relative body weight are depicted in the right panel. F, BxPC-3-GPC1-KO cell viability after treatment with the conditioned medium from the humanized GPC1-ADC-treated BxPC-3 cells. G, Conditioned media generated by exposing the BxPC-3 cells with the control-ADC or humanized GPC1-ADC for 48 h. After 144 h, the cell viability was determined.

Table 1

IC₅₀ values of humanized GPC1-ADC and MMAE in pancreatic cancer and esophageal squamous cell carcinoma cell lines.

Cell Lines	GPC1 expression (ABC/cell)	Humanized GPC1-ADC (nM)	Control-ADC (nM)	MMAE (nM)
BxPC-3	93,290	0.235	N.D.	0.310
KP-2	262,409	0.0383	N.D.	0.288
PK-8	129,630	0.228	N.D.	0.334
TE8	249,304	0.0666	N.D.	0.304
TE14	219,581	0.291	N.D.	0.296
KYSE70	112,247	0.343	N.D.	0.349
BxPC-3 GPC1-KO	N.D.	N.D.	N.D.	0.317
TE8 GPC1-KO	N.D.	N.D.	N.D.	0.336

ABC, antibody binding capacity; ADC, antibody-drug conjugate; GPC1, glypican-1; MMAE, monomethyl auristatin E; N.D., none detected

The GPC1-positive BxPC-3 xenograft model was designed to assess the ability of the humanized GPC1-ADC(MMAE) to mediate antitumor activity. The humanized GPC1-ADC(MMAE) significantly and dose-dependently suppressed the tumor growth as compared with PBS and control-ADC(MMAE) (Fig. 3B).

The BxPC-3-GPC1-KO-Luc#15 xenograft model was used as a negative control. The SCID mice were subcutaneously inoculated with BxPC-3-GPC1-KO-Luc#15 cells and then intravenously treated with PBS, 10-mg/kg control-ADC, or 10-mg/kg humanized GPC1-ADC(MMAE) twice a week for a total of four times. The humanized GPC1-ADC(MMAE) had no effect on the GPC1-negative model. Both the humanized GPC1-ADC(MMAE) and control-ADC(MMAE) slightly suppressed the tumor growth as compared with PBS, but no significant difference was found between the three groups (Fig. 3C).

As described earlier, the antitumor activity of the humanized GPC1-ADC(MMAE) was evaluated against a GPC1-positive (using BxPC-3) or GPC1-negative model (using BxPC-3-GPC1-KO-Luc#15). We found that the humanized GPC1-ADC(MMAE) showed a tumor growth inhibitory effect on the GPC1-positive cells but not on the GPC1-negative cells alone. Considering that the MMAE released from the humanized GPC1-ADC(MMAE) possesses a high cell-membrane permeable activity and bystander killing effect, the humanized GPC1-ADC(MMAE) should also be effective for GPC1-negative cells adjacent to the GPC1-positive cells. To verify the bystander killing effect of humanized GPC1-ADC(MMAE), a co-inoculation xenograft model was used. As shown in Figure 3A, we confirmed the heterogeneity of the mixed tumor generated by inoculating a mixture of BxPC3 and BxPC3-GPC1-KO-Luc#15. PBS, control-ADC(MMAE), or humanized GPC1-ADC(MMAE) was intravenously administered to the co-inoculated xenograft mice, and the tumor volume and luciferase activity were measured. The humanized GPC1-ADC(MMAE) significantly suppressed the tumor growth and luciferase signal as compared with the PBS and control-ADC(MMAE), indicating that the BxPC-3-GPC1-KO-Luc#15 cells were damaged by the bystander killing effect of MMAE that was derived from the humanized GPC1-ADC(MMAE) (Fig. 3D-E). In each experiment, no significant weight loss was observed in any group (Fig. 3E).

We also assessed the bystander activity of the humanized GPC1-ADC(MMAE) *in vitro* as illustrated in Figure 3F, using GPC1-positive BxPC-3 and GPC1-negative BxPC-3-GPC1-KO cells. The humanized GPC1-ADC(MMAE) or control-ADC(MMAE) was exposed to the BxPC-3 cells for 48 h, and culture medium (CM) was transferred to the BxPC-3-GPC1-KO cells. The CM from BxPC-3 treated with GPC1-ADC(MMAE) caused a dose-dependent decrease in BxPC-3-GPC1-KO viability (Fig. 3G).

In vivo efficacy study of humanized GPC1-ADC(MMAE) in the pancreatic cancer liver metastases xenograft model

Liver metastasis is frequently observed in PDAC and associated with a poor prognosis. To assess whether the GPC1 expression was retained in the liver metastasis of PDAC, IHC analysis was performed. The GPC1 expression was detected both in the matched primary tumor and liver metastasis of PDAC (Fig. 4A). The retained expression of the GPC1 primary tumors and metastases led us to hypothesize that the humanized GPC1-ADC(MMAE) may also elicit an activity against preestablished metastases.

To demonstrate the efficacy of the humanized GPC1-ADC(MMAE) against the liver metastasis of PDAC, preclinically established experimental metastasis was used. BxPC-3-Luc#2 cells were inoculated intrasplenically to produce pancreatic cancer liver metastases. By IHC analysis, liver metastasis was successfully produced using BxPC-3-Luc#2 cells (Fig. 4B). The mice were randomized into two groups of equal average tumor burden based on the luciferase activity, 7 to 14 days post-inoculation. Vehicle or humanized GPC1-ADC(MMAE) (10 mg/kg) was administered (twice a week for two weeks). We revealed that the humanized GPC1-ADC(MMAE) significantly reduced the tumor burden ($P < 0.01$) as compared with the vehicle treatment and no significant weight loss was observed in humanized GPC1-ADC(MMAE) administered group compared to vehicle (Fig. 4C-D). Furthermore, humanized GPC1-ADC(MMAE) significantly prolonged survival ($P < 0.0001$) compared to vehicle treatment (Fig. 4E).

Humanized GPC1-ADC(MMAE) showed a potent tumor growth inhibition in the pancreatic ductal adenocarcinoma and esophageal squamous cell carcinoma patient-derived xenograft models

We also evaluated the therapeutic effects of the humanized GPC1-ADC(MMAE) on PDAC and ESCC *in vivo* using PDX models. Tumor tissues were subcutaneously implanted in NOG mice. The mice then received intravenous 1-, 3-, or 10-mg/kg GPC1-ADC once a week for a total of 4 times (Fig. 5). The GPC1 expressions in the tumor tissues were confirmed by IHC. In the PDAC PDX models (PK565, PK175, and KPK1), humanized GPC1-ADC(MMAE) significantly suppressed the tumor growth as compared with PBS and control-ADC (Fig. 5A-C). In particular, 10-mg/kg humanized GPC1-ADC suppressed the tumor growth to almost flat. In the ESCC PDX models (ESCC14 and ESCC2), the humanized GPC1-ADC(MMAE) showed a potent therapeutic effect (Fig. 5D-E). Tumor growth was significantly suppressed in the humanized GPC1-ADC(MMAE) group, and the tumors almost disappeared in the 3- and 10-mg/kg humanized GPC1-ADC(MMAE) groups. No significant

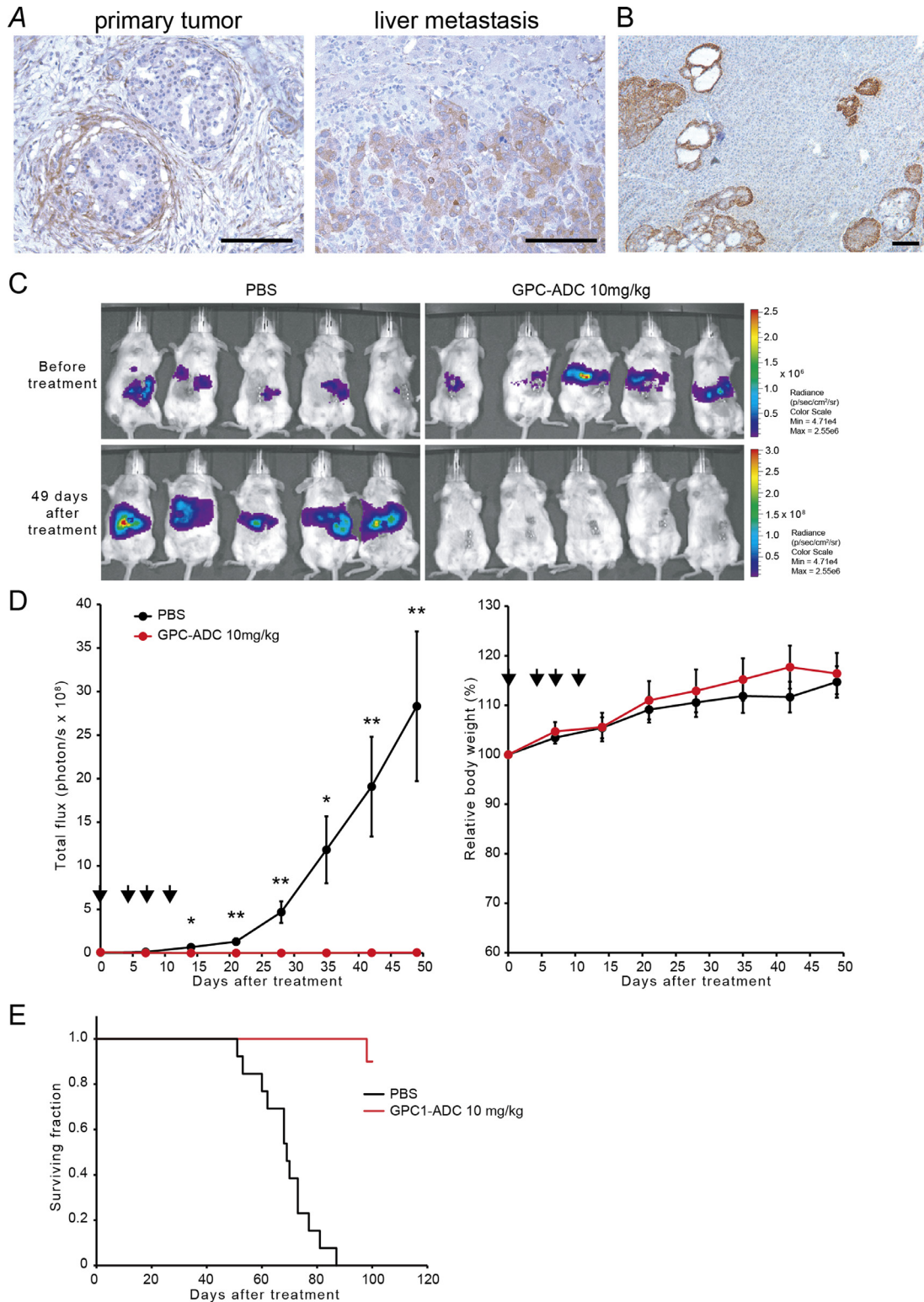


Fig. 4. Antitumor activity of the humanized GPC1-ADC(MMAE) in the pancreatic cancer liver metastasis xenograft model
 A, Representative images of IHC staining for GPC1 in tumor tissues in the matched primary and liver metastases of a patient with PDAC. Scale bar: 100 μ m.
 B, Representative images of IHC staining for GPC1 in BxPC-3-Luc#2 pancreatic cancer liver metastases after intrasplenic injection of tumor cells are shown. Scale bar: 100 μ m.
 C, The humanized GPC1-ADC(MMAE) inhibits the BxPC-3-Luc#2 pancreatic cancer liver metastases in the mice after intrasplenic injection of tumor cells. BLI was used to monitor the BxPC-3-Luc#2 pancreatic cancer liver metastases in the mice after intrasplenic injection of cancer cells. BLI was used 7 to 14 days post-inoculation to randomize the mice into vehicle ($n = 13$) or 10-mg/kg humanized GPC1-ADC(MMAE) treatment groups ($n = 10$). Note the decrease in bioluminescence in the humanized GPC1-ADC(MMAE)-treated group at 49 days post-inoculation.
 D, Quantification of the tumor burden from the BxPC-3-Luc#2 liver metastasis study shown in C. Changes in relative body weight. The error bars denote the SEM.
 E, Kaplan-Meier survival analysis of the BxPC-3-Luc#2 liver metastasis study shown in C. Log-rank analysis: $p < 0.0001$, humanized GPC1-ADC(MMAE) versus vehicle.

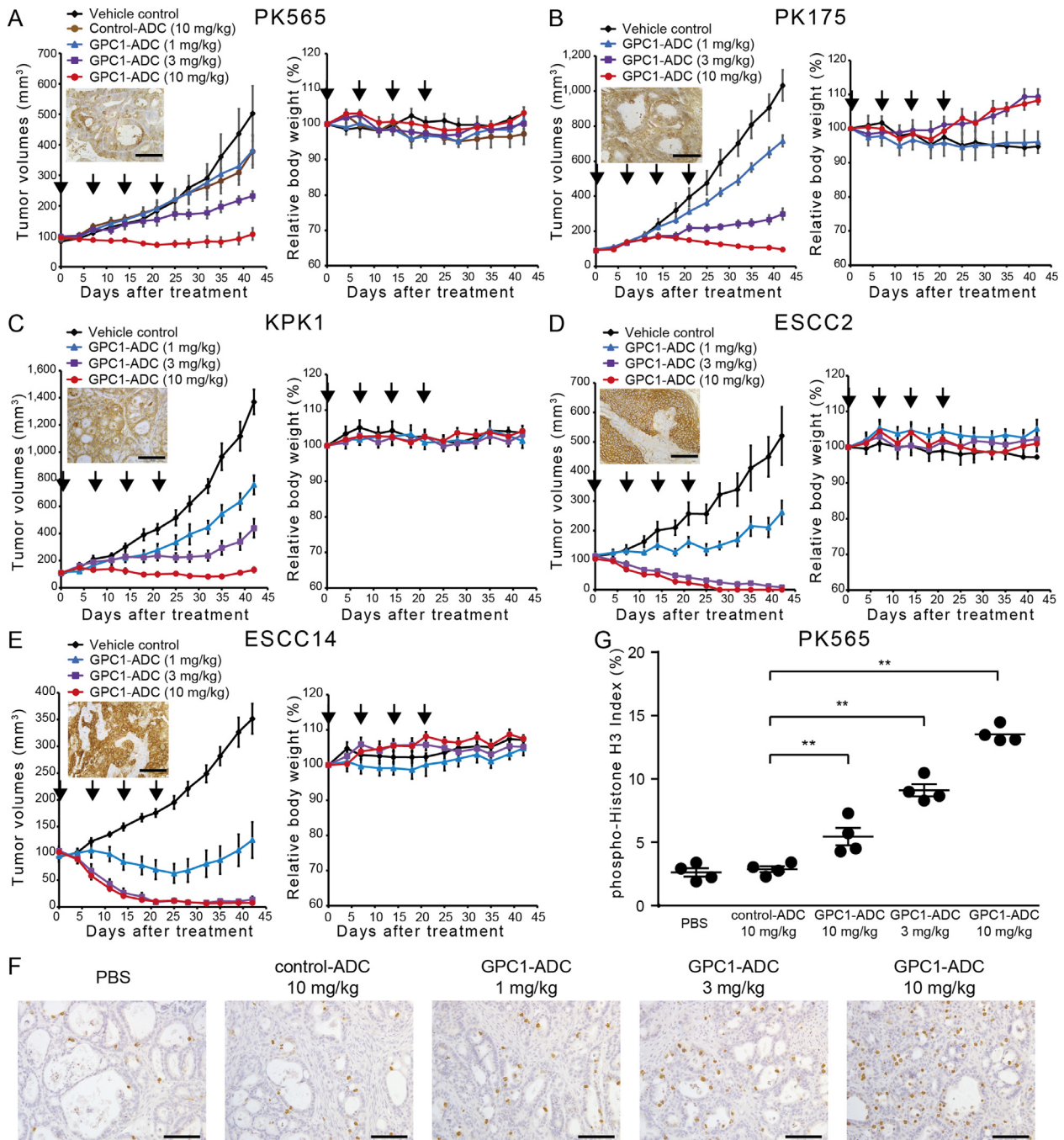


Fig. 5. Antitumor activity of the humanized GPC1-ADC(MMAE) in the pancreatic cancer and ESCC PDX models

A-E, Antitumor efficacy of the humanized GPC1-ADC(MMAE) in the PK565, PK175, KPK1, ESCC2, and ESCC14 PDX models ($n = 7-8$ per group). Representative images of IHC staining for GPC1 in xenografted tumor tissues from untreated mice are inserted. Scale bar: 100 μ m. The tumor-bearing mice were given PBS, control-ADC(MMAE) (10 mg/kg), or humanized GPC1-ADC(MMAE) (1, 3, and 10 mg/kg) intravenously on days 0, 7, 14, and 21. Each point on the graph represents the average tumor volume. Changes in body weight are also represented. F, Humanized GPC1-ADC causes mitotic arrest *in vivo*. Animals bearing the PK565 tumor xenografts are given a single dose of PBS, control-ADC(MMAE) (10 mg/kg), or humanized GPC1-ADC(MMAE) (10 mg/kg). After 24 h, the tumors were harvested and stained with an anti-phospho-histone H3 (Ser10) antibody to detect mitotic cells. Scale bar: 100 μ m. G Phospho-histone H3 (Ser10) staining was assessed as the ratio of mitotic cells to the total number of tumor cells in 4 fields (magnification, $\times 200$). $**P < 0.01$, one-way ANOVA, followed by Dunnett's post hoc test.

weight loss was observed in any group (Fig. 5). To analyze the pharmacologic action of humanized GPC1-ADC(MMAE) *in vivo*, IHC staining of PK565 PDX tumors with anti-phosphorylated histone H3 (Ser10) antibody, which is a marker of mitosis, was performed. There was an increase in mitotic cells following treatment with humanized GPC1-ADC(MMAE), but not with control-ADC(MMAE) (Fig. 5F). The percentage of mitotic cells was significantly increased in 1 mg/kg, 3 mg/kg, and 10 mg/kg humanized GPC1-ADC(MMAE) administered group compared with the control-ADC(MMAE) administered group ($P < 0.01$; Fig. 5G). These findings suggest that the tubulin polymerizing inhibitor, MMAE, was effectively delivered to the tumor cells of PK565 by the anti-GPC1 mAb and caused mitotic arrest.

Discussion

PDAC and ESCC represent a significant global health problem; thus, there is an urgent need for the development of a more effective agent to control these diseases. A large proportion of these tumors have been shown to overexpress GPC1 [14,18,19,24-26]. The overexpression of GPC1 in PDAC was confirmed by detailed IHC studies. GPC1 expression has been demonstrated to be retained in the liver metastases of patients with PDAC (Fig. 4). Lu *et al.* reported that GPC1 overexpression was detected in tumor metastases to the lymph nodes, abdominal wall, and liver in patients with PDAC [26]. Moreover, the limited GPC1 expression in normal human tissues certifies GPC1 as an attractive candidate target of antibody-based cancer therapy.

In this study, the humanized anti-GPC1 antibody clone T2 was generated by humanizing the mouse anti-GPC1 monoclonal antibody clone 01a033. We demonstrated the detailed preclinical characterization of the humanized anti-GPC1 antibody clone T2 conjugated to the tubulin inhibitor MMAE and humanized GPC1-ADC(MMAE), targeting GPC1-expressing tumors.

The efficacy of an ADC predominantly depends on the expression of the target antigen, ADC-binding affinity and subsequent internalization within the cells, and the potency of the conjugated payload. Our data demonstrate that the humanized anti-GPC1 antibody clone T2 possesses a specific nanomolar-binding affinity for human GPC1 and undergoes a subsequent internalization. The binding properties are not altered and retained in the humanized GPC1-ADC(MMAE) (Fig. 1).

Humanized GPC1-ADC(MMAE) is shown to be both potent and highly selective in killing GPC1-expressing tumor cells, whereas the same dose range does not affect GPC1-negative cells. The mode of action of humanized GPC1-ADC(MMAE) includes cycle arrest in the G2/M phase and apoptosis through caspase3/7 dependent pathway. MMAE, the tubulin-binding payload, mainly acts on proliferating cells and therefore provides further functional specificity to the ADC beyond the specific target binding of the antibody moiety.

Furthermore, the treatment of the mice bearing either GPC1-negative or GPC1-positive tumors with humanized GPC1-ADC(MMAE) or a nontargeted control-ADC harboring the same linker payload, respectively, indicates that the target-independent antitumor effects are only minor when compared with the targeted activity of the humanized GPC1-ADC(MMAE). The inferior target-independent *in vivo* effects of the control-ADC at high doses are presumably due to enhanced permeability and retention (EPR) in solid tumors. This phenomenon of passive drug targeting of tumors has been widely described for macromolecules and lipids [27].

Once humanized GPC1-ADC(MMAE) is bound and internalized by a tumor cell, degradation of the humanized GPC1-ADC(MMAE) peptide linker releases a cell-permeable payload metabolite with bystander killing potential [21]. This bystander effect was demonstrated *in vitro* and *in vivo* by using a xenograft model using co-culture of GPC1-positive and GPC1-negative cells within the inoculated tumors (Fig. 3). Humanized GPC1-

ADC(MMAE) not only inhibited tumor growth but also induced tumor regression. This strongly suggests that in addition to the EPR effect observed in the GPC1-negative cells, the bystander effect contributes to the antitumor activity of the humanized GPC1-ADC(MMAE).

In addition to the subcutaneous and liver metastatic xenograft tumor models, we further demonstrated the dose-dependent therapeutic activity of the humanized GPC1-ADC(MMAE) in PDX tumors that more closely mimic human tumor characteristics such as heterogeneity. Treatment with humanized GPC1-ADC(MMAE) resulted in the total eradication of established tumors with no tumor recurrence and was reproducible in several models over a long observational period, further indicating complete tumor cell elimination by the ADC.

Based on our findings on the BxPC-3 liver metastases model, we expect that humanized GPC1-ADC(MMAE) may improve survival of patients with advanced PDAC by restraining established liver metastases. Interestingly, a recent study has shown that GPC1 contributes to metastasis of renal carcinoma cells [28]. At present, our data only showed that humanized GPC1-ADC(MMAE) directly damages metastasized tumor cells in the liver. Further study is necessary to examine whether treatment with humanized GPC1-ADC(MMAE) can inhibit the formation of metastatic lesions.

Our group initially used a naked anti-GPC1 antibody (clone 1-12) to treat PDX models. Although the naked antibody (clone 1-12) inhibited tumor growth in the esophageal cancer ESCC8 PDX model mainly via the ADCC and CDC activity [14], it was ineffective in the BxPC-3 xenograft model [19]. The reason for this difference remains unknown but is likely explained by the findings that GPC1 expression levels are typically lower in PDAC than in ESCC. We then generated another anti-GPC1 monoclonal antibody (clone 01a033), a parent clone of humanized GPC1 monoclonal antibody (clone T2), which has a high internalizing activity suitable for ADC [17]. Using the clone 01a033, we developed GPC1-ADC and showed that this ADC strongly inhibited the tumor growth in the BxPC-3 xenograft model [19]. These results demonstrate that GPC1-ADC has the advantage over the naked antibody by exerting direct killing effect on GPC1-positive tumor cells including those with relatively low GPC1 expression.

Humanized GPC1-ADC(MMAE) may have weaknesses due to its potent killing activity on GPC1-positive cells. For example, it has been reported that GPC1 is expressed on vascular endothelial cells [29], raising the question of whether humanized GPC1-ADC(MMAE) might show a toxic effect on vascular endothelial cells. It should be noted that MMAE is known to be recognized as a substrate by multidrug resistance-1 (MDR-1) [30], which is highly expressed in vascular endothelial cells. Thus, even humanized GPC1-ADC(MMAE) is incorporated into the GPC1-positive vascular endothelial cells, intracellularly released MMAE would be efficiently effluxed by MDR-1 [31]. In addition, we used human IgG4, a subclass lacking ADCC and CDC activity, to generate the humanized anti-GPC1 antibody. Thus, humanized GPC1-ADC(MMAE) may show little toxicity to vascular endothelial cells, although this should be evaluated very carefully in future clinical studies.

Taken together, our preclinical results validate GPC1 as a cancer antigen for ADC as a potential therapeutic approach. Future studies are needed to determine the threshold of the GPC1 expression required to achieve efficient ADC-induced antitumor efficacy. This information is crucial for developing companion diagnostics to stratify patient populations in clinical development.

Data availability

All data generated or analyzed during this study are included in this published article and its supplementary information files.

Consent for publication

Not applicable.

Authors' contributions

Conception and design: Satoshi Serada and Tetsuji Naka.

Methodology development: Eri Munekage, Satoshi Serada, Shigehiro Tsujii.

Data acquisition: Eri Munekage, Satoshi Serada, Shigehiro Tsujii, Keiichiro Yokota, Keita Kiuchi, Kenji Tominaga.

Patient-derived xenograft: Taisei Nomura.

Data analysis and interpretation: Eri Munekage, Satoshi Serada, Shigehiro Tsujii, Keiichiro Yokota, Keita Kiuchi, Kenji Tominaga, Minoru Fujimoto, Mizuki Kanda, Sunao Uemura, Tsutomu Namikawa, Ichiro Murakami, Kazuhiro Hanazaki, Tetsuji Naka.

Manuscript writing, review, and/or revision: Eri Munekage, Satoshi Serada, Shigehiro Tsujii, Kazuhiro Hanazaki, Tetsuji Naka.

Administrative, technical, or material support: Satoshi Serada.

Study supervision: Tetsuji Naka.

Acknowledgments

We would like to thank M. Arimitsu, C. Negayama for their secretarial assistance. We also thank A. Yamamoto for her technical assistance.

Supplementary materials

Supplementary material associated with this article can be found, in the online version, at doi:10.1016/j.neo.2021.07.006.

References

- [1] Rawla P, Sunkara T, Gaduputi V. Epidemiology of pancreatic cancer: global trends. *World J Oncol* 2019;**10**:10–27.
- [2] Rahib L, Smith BD, Aizenberg R, Rosenzweig AB, Fleshman JM, Matrisian LM. Projecting cancer incidence and deaths to 2030: the unexpected burden of thyroid, liver, and pancreas cancers in the United States. *Cancer Res* 2014;**74**:2913–21.
- [3] Ilic M, Ilic I. Epidemiology of pancreatic cancer. *World J Gastroenterol* 2016;**22**:9694–705.
- [4] Uhlenhopp DJ, Then EO, Sunkara T, Gaduputi V. Epidemiology of esophageal cancer: update in global trends, etiology and risk factors. *Clin J Gastroenterol* 2020;**6**:1010–21.
- [5] Katz J, Janik JE, Younes A. Brentuximab Vedotin (SGN-35). *Clin Cancer Res* 2011;**17**:6428–36.
- [6] Younes A, Gopal AK, Smith SE, Ansell SM, Rosenblatt JD, Savage KJ, Ramchandren R, Bartlett NL, Cheson BD, de Vos S. Results of a pivotal phase II study of brentuximab vedotin for patients with relapsed or refractory Hodgkin's lymphoma. *J Clin Oncol* 2012;**30**:2183–9.
- [7] Burris HA 3rd, Rugo HS, Vukelja SJ, Vogel CL, Borson RA, Limentani S, Tan-Chiu E, Krop IE, Michaelson RA, Girish S. Phase II study of the antibody drug conjugate trastuzumab-DM1 for the treatment of human epidermal growth factor receptor 2 (HER2)-positive breast cancer after prior HER2-directed therapy. *J Clin Oncol* 2011;**29**:398–405.
- [8] LoRusso PM, Weiss D, Guardino E, Girish S, Sliwkowski MX. Trastuzumab emtansine: a unique antibody-drug conjugate in development for human epidermal growth factor receptor 2-positive cancer. *Clin Cancer Res* 2011;**17**:6437–47.
- [9] Krop IE, LoRusso P, Miller KD, Modi S, Yardley D, Rodriguez G, Guardino E, Lu M, Zheng M, Girish S. A phase II study of trastuzumab emtansine in patients with human epidermal growth factor receptor 2-positive metastatic breast cancer who were previously treated with trastuzumab, lapatinib, an anthracycline, a taxane, and capecitabine. *J Clin Oncol* 2012;**30**:3234–41.
- [10] Hara H, Takahashi T, Serada S, Fujimoto M, Ohkawara T, Nakatsuka R, Harada E, Nishigaki T, Takahashi Y, Nojima S. Overexpression of glypican-1 implicates poor prognosis and their chemoresistance in oesophageal squamous cell carcinoma. *Br J Cancer* 2016;**115**:66–75.
- [11] Filmus J, Selleck SB. Glypicans: proteoglycans with a surprise. *J Clin Invest* 2001;**108**:497–501.
- [12] Filmus J, Capurro M, Rast J. Glypicans. *Genome Biol* 2008;**9**:224.
- [13] Lund ME, Campbell DH, Walsh BJ. The role of glypican-1 in the tumor microenvironment. *Adv Exp Med Biol* 2020;**1245**:163–76.
- [14] Harada E, Serada S, Fujimoto M, Takahashi Y, Takahashi T, Hara H, Nakatsuka R, Sugase T, Nishigaki T, Saito Y. Glypican-1 targeted antibody-based therapy induces preclinical antitumor activity against esophageal squamous cell carcinoma. *Oncotarget* 2017;**8**:24741–52.
- [15] Matsuda K, Maruyama H, Guo F, Kleeff J, Itakura J, Matsumoto Y, Lander AD, Korc M. Glypican-1 is overexpressed in human breast cancer and modulates the mitogenic effects of multiple heparin-binding growth factors in breast cancer cells. *Cancer Res* 2001;**61**:5562–9.
- [16] Qiao D, Meyer K, Mundhenke C, Drew SA, Friedl A. Heparan sulfate proteoglycans as regulators of fibroblast growth factor-2 signaling in brain endothelial cells. Specific role for glypican-1 in glioma angiogenesis. *J Biol Chem* 2003;**278**:16045–53.
- [17] Matsuzaki S, Serada S, Hiramatsu K, Nojima S, Ueda Y, Ohkawara T, Mabuchi S, Fujimoto M, Morii E, Yoshino K. Anti-glypican-1 antibody-drug conjugate exhibits potent preclinical antitumor activity against glypican-1 positive uterine cervical cancer. *Int J Cancer* 2018;**142**:1056–66.
- [18] Kleeff J, Ishiwata T, Kumbasar A, Friess H, Buchler MW, Lander AD, Korc M. The cell-surface heparan sulfate proteoglycan glypican-1 regulates growth factor action in pancreatic carcinoma cells and is overexpressed in human pancreatic cancer. *J Clin Invest* 1998;**102**:1662–73.
- [19] Nishigaki T, Takahashi T, Serada S, Fujimoto M, Ohkawara T, Hara H, Sugase T, Otsuru T, Saito Y, Tsujii S. Anti-glypican-1 antibody-drug conjugate is a potential therapy against pancreatic cancer. *Br J Cancer* 2020;**122**:1333–41.
- [20] Okeley NM, Miyamoto JB, Zhang X, Sanderson RJ, Benjamin DR, Sievers EL, Senter PD, Alley SC. Intracellular activation of SGN-35, a potent anti-CD30 antibody-drug conjugate. *Clin Cancer Res* 2010;**16**:888–97.
- [21] Sztot C, Saha S, Zhang XM, Zhu Z, Hilton MB, Morris K, Seaman S, Dunleavy JM, Hsu KS, Yu GJ. Tumor stroma-targeted antibody-drug conjugate triggers localized anticancer drug release. *J Clin Invest* 2018;**128**:2927–43.
- [22] Yokoyama T, Enomoto T, Serada S, Morimoto A, Matsuzaki S, Ueda Y, Yoshino K, Fujita M, Kyo S, Iwahori K. Plasma membrane proteomics identifies bone marrow stromal antigen 2 as a potential therapeutic target in endometrial cancer. *Int J Cancer* 2013;**132**:472–84.
- [23] Doronina SO, Mendelsohn BA, Bovee TD, Cerveny CG, Alley SC, Meyer DL, Oflazoglu E, Toki BE, Sanderson RJ, Zabinski RF. Enhanced activity of monomethylauristatin F through monoclonal antibody delivery: effects of linker technology on efficacy and toxicity. *Bioconjug Chem* 2006;**17**:114–24.
- [24] Duan L, Hu XQ, Feng DY, Lei SY, Hu GH. GPC-1 may serve as a predictor of perineural invasion and a prognosticator of survival in pancreatic cancer. *Asian J Surg* 2013;**36**:7–12.
- [25] Tanaka M, Ishikawa S, Ushiku T, Morikawa T, Isagawa T, Yamagishi M, Yamamoto H, Katoh H, Takeshita K, Arita J. EVI1 modulates oncogenic role of GPC1 in pancreatic carcinogenesis. *Oncotarget* 2017;**8**:99552–66.
- [26] Lu H, Niu F, Liu F, Gao J, Sun Y, Zhao X. Elevated glypican-1 expression is associated with an unfavorable prognosis in pancreatic ductal adenocarcinoma. *Cancer Med* 2017;**6**:1181–91.
- [27] Maeda H. The enhanced permeability and retention (EPR) effect in tumor vasculature: the key role of tumor-selective macromolecular drug targeting. *Adv Enzyme Regul* 2001;**41**:189–207.
- [28] Moran H, Cancel LM, Mayer MA, Qazi H, Munn LL, Tarbell JM. The cancer cell glycocalyx proteoglycan Glypican-1 mediates interstitial flow mechanotransduction to enhance cell migration and metastasis. *Biorheology* 2019;**56**:151–61.
- [29] Potje SR, Paula TD, Paulo M, Bendhack LM. The role of glycocalyx and caveolae in vascular homeostasis and diseases. *Front Physiol* 2020;**11**:620840.

- [30] Chen R, Hou J, Newman E, Kim Y, Donohue C, Liu X, Thomas SH, Forman SJ, Kane SE. CD30 Downregulation, MMAE Resistance, and MDR1 upregulation are all associated with resistance to brentuximab Vedotin. *Mol Cancer Ther* 2015;**14**:1376–84.
- [31] Seaman S, Zhu Z, Saha S, Zhang XM, Yang MY, Hilton MB, Morris K, Szot C, Morris H, Swing DA. Eradication of tumors through simultaneous ablation of cd276/b7-h3-positive tumor cells and tumor vasculature. *Cancer Cell* 2017;**31**:501–15.